Batteries & Supercaps

Research Article
doi.org/10.1002/batt.202200426

Chemistry
Europe
European Chemical
Societies Publishing

www.batteries-supercaps.org

A PEGylated Viologen for Crossover-Free and High-Capacity pH-Neutral Aqueous Organic Redox Flow Batteries

Kang Peng+,[a] Pan Sun+,[a] Zhengjin Yang,*[a] and Tongwen Xu*[a]

Aqueous organic redox flow batteries (AORFBs), which exploit the reversible electrochemical reactions of water soluble organic electrolytes to store electricity, gain increasing momentum for the grid-scale integration of renewable electricity. However, the crossover of organic electrolytes across the membrane and the limited capacity significantly impede the widespread adoption of AORFBs. Here we report a PEGylated viologen anolyte bearing four positive charges, namely BTMAE–Vi, for crossover-free and high capacity pH-neutral AORFBs. This anolyte is rationally designed by appending positively charged ethylene glycol side chains to raise water solubility and increase the molecular size. The solubility of BTMAE–Vi is increased to 3.4 M because of an improved molecular polarity and the existence of four positive charges, while membrane crossover rate is significantly reduced. A BTMAE–Vi-based flow cell demonstrates an extremely high capacity retention rate of 99.996% per cycle or 99.979% per hour when the first reversible redox reaction is utilized, but the irreversible molecular decomposition of the doubly reduced BTMAE–Vi results in severe capacity fade. Our results and the proposed concept in mitigating membrane crossover and elevating capacity will pave the way for developing high-performance AORFBs.

Introduction

To limit climate warming and environment worsening, photovoltaic and wind-based electricity are drawing increasing attention as potential replacements for conventional fossil fuels because of their clean and abundant nature.[1] However, the intrinsic intermittency of these renewable energy sources impedes their widespread application.[2] This conundrum may be solved by redox flow batteries, which feature low cost, high safety, design flexibility and scalability. They are deemed as an efficient option for resolving energy supply and demand imbalances. Especially promising is the aqueous organic redox flow battery (AORFB), which takes advantage of the reversible redox reactions of water-soluble organic materials to store energy.[3] The structure tunability of organic materials may endow electrolytes with fast redox kinetics, high solubility, and high stability through proper chemical modifications.[4]

Presently, available electrolytes of AORFBs include quinones, viologens, nitroxide radicals, aza-aromatics, and organometallics.[5] As anolytes, viologen derivatives merit low cost, reversible electrochemical reactions, fast redox kinetics, and high water solubility and can be operated in neutral aqueous solutions that are non-corrosive and nonflammable.

They are gaining wide attention from both the academic and the industrial community. Liu et al.[6] were the first to report methyl viologen (MV) as anolyte for AORFBs. MV is easily synthesized and has high water solubility (3.0 M). However, when combined with 4-OH-TEMPO as catholyte, the MV/4-OH-TEMPO battery demonstrated fast capacity loss of 3.6% per day because of the dimerization of redox intermediate and cross-membrane contamination. Bis(trimethylammoniopropyl) functionalized viologen, namely BTMAP–Vi, was proposed to restrict the dimerization and block crossover through anion exchange membranes because of the enhanced charge repulsion.[7a] Furthermore, bis (3-trimethylammonio-2-hydroxy)propyl viologen tetrachloride, namely Dex-Vi, was designed by Feng et al.,[7b] exhibiting ultralow anion-exchange membrane permeability, high volumetric capacity capability, and outstanding chemical stability. Similarly, sulfonate-functionalized viologen molecule, namely $(SPr)_2V$, was proposed and demonstrated obvious charge repulsion and size exclusion, being particularly compatible with cation exchange membranes.[8] In addition, Aziz et al.[9a] presented a phosphonate-substituted viologen, namely BPP–Vi, which is less susceptible to bimolecular decomposition and has very low permeation rate through a cation exchange membrane because of strong charge repulsion. Very recently, Wang et al.[9b] reported a phosphonate functionalized phenylene-bridged viologen derivative, namely $(PPBPy)Br_2$, which has a relatively low redox potential.

Although enormous efforts have been devoted recently to modify viologen,[10] the cross-membrane-contamination remains a ubiquitous issue in AORFBs, resulting in inferior cyclability. Even if the crossover contamination is controlled at a low level in some cases, the previously reported molecule modifying strategies decrease the water solubility of the pristine viologen derivatives. Therefore, ensuring high water

[a] K. Peng,+ P. Sun,+ Prof. Z. Yang, Prof. T. Xu
Department of Applied Chemistry,
School of Chemistry and Materials Science
University of Science and Technology of China
Hefei 230026, P.R. China
E-mail: yangzj09@ustc.edu.cn
      twxu@ustc.edu.cn
[+] These authors contributed equally to this work.

An invited contribution to a Special Collection on Organic Batteries.

Batteries & Supercaps

Research Article
doi.org/10.1002/batt.202200426

Chemistry
Europe
European Chemical
Societies Publishing

solubility while mitigating the membrane crossover of viologen derivatives remains a challenge.

In this study, we report a PEGylated viologen with four positive charges, BTMAE–Vi, synthesized from low-cost 4,4'-bipyridine. The introduction of long ethylene glycol trimethyl ammonium side chains increases size, polarity, and the number of positive charge of the molecule, as compared to MV, thereby significantly mitigating molecular crossover through membranes and improving its solubility in water (3.4 M). BTMAE–Vi can undergo a two-electron redox process, with fast redox kinetics. When combined with (ferrocenylmethyl)trimethylammonium chloride (FcNCl), the cell operated in pH-neutral conditions demonstrates an open-circuit voltage of 1.37 V and a peak power density of 127.83 mW cm^{-2}. When BTMAE–Vi undergoes a two-electron charging/discharging, the FcNCl/BTMAE–Vi cell demonstrates a capacity retention rate of 99.893% per cycle. The doubly reduced BTMAE–Vi undergoes irreversible molecular decomposition as revealed by a combined framework post-analysis, symmetric cell cycling, and computational simulation, causing capacity fade. In contrast, an extremely high capacity retention rate of 99.996% per cycle or 99.979% per hour is achieved when BTMAE–Vi undergoes a one-electron charging/discharging. During extended cell cy-

cling, no crossover of BTMAE–Vi to the catholyte solution was detected.

Results and Discussion

The synthetic route of BTMAE–Vi is illustrated in Figure 1(a). And the structures of 2-(2-(2-chloroethoxy)ethyl)-trimethyl-ammonium chloride and BTMAE-Vi were verified by ^{1}H NMR spectra in Figures S1 and S2, respectively. The electrochemical properties of BTMAE–Vi were then evaluated using cyclic voltammetry (CV) and rotating disk electrodes (RDE). The CV curves show that BTMAE–Vi undergoes two fully reversible one-electron redox processes, with redox potentials of -0.40 and -0.74 V versus standard hydrogen electrode (SHE) (Figure 1b). The anodic-cathodic peak separations remain constant, while the plots of the peak currents as a function of the square roots of scan rates exhibit strict linear relationships (Figure S3), indicating that both redox steps are diffusion controlled.[11] The diffusion coefficients (D) of BTMAE–Vi were calculated using the RDE method to be 3.6×10^{-6} and 3.3×10^{-6} cm^2 s^{-1} for its first and second electro-reductions, respectively (Figure 1c and d). In addition, according to the Levich equation and the Butler-Volmer equation,[12] the values of electron transfer rate
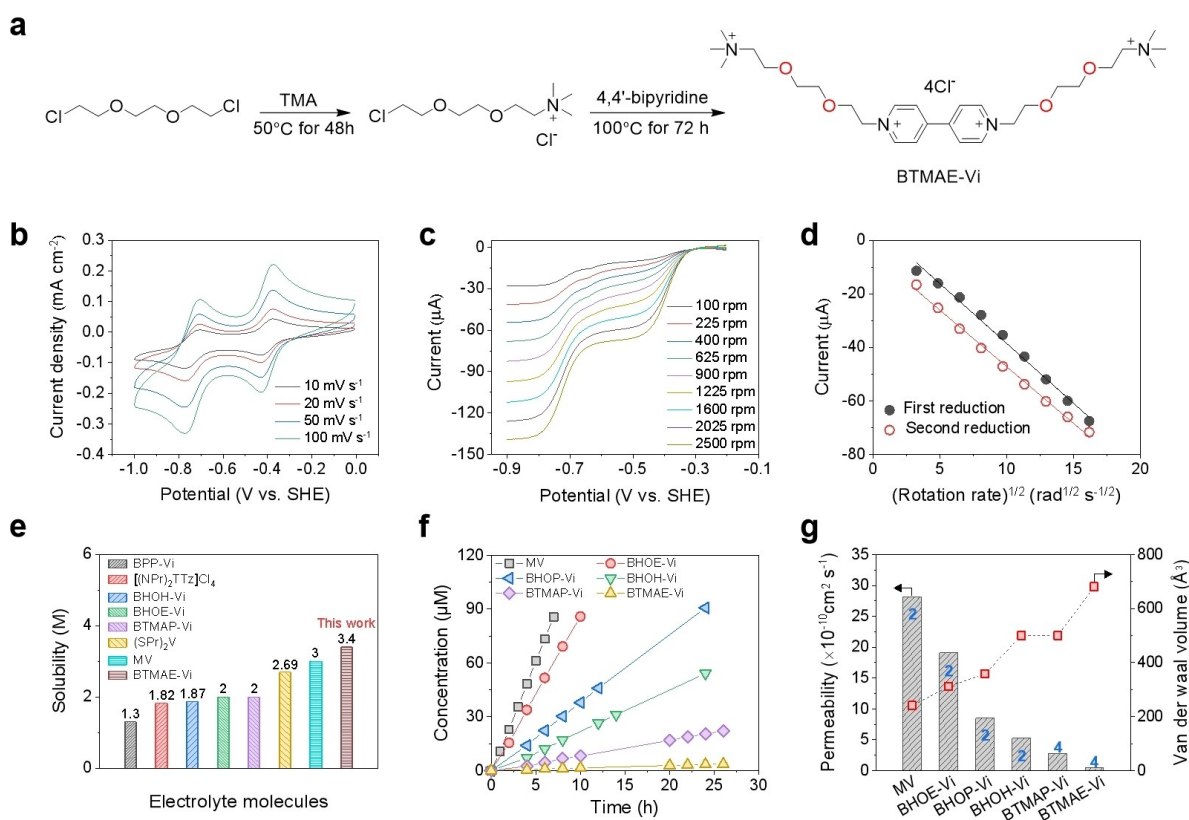

Figure 1. a) The synthetic route of BTMAE–Vi. b) Cyclic voltammograms of 1.0 mM BTMAE–Vi dissolved in 1.0 M NaCl aqueous solution at varying potential scanning rates, with glassy carbon as the working electrode. c) RDE measurements of 1.0 mM BTMAE–Vi dissolved in 1.0 M NaCl aqueous solution with a potential scanning rate of 10 mV s^{-1} at rotating speeds between 100 and 2500 rpm. d) Levich plot of the limiting currents as a function of the square root of the rotating speeds. e) The solubility of different viologen derivatives in water. The values are compared with those reported by literatures.[6–9,14] f) The permeation rate of different viologen derivatives across a commercial Selemion DSV membrane in a two-compartment diffusion cell. g) Permeability and Van der Waal volume of different viologen derivatives. The number of charges is marked in blue for all the molecules.

constants (k_0) were determined to be 1.1×10^{-2} and $1.2 \times 10^{-2} \, cm \, s^{-1}$ for the first and second reductions, respectively (Figure S4), both of which are greater than most of the inorganic, organic, or organometallic species.[13]

The water solubility of BTMAE–Vi was measured through UV−Vis spectrophotometry method, showing a maximum water solubility of 3.4 M. The solubility of BTMAE–Vi is higher than other viologen-based organics[6–9,14] (Figure 1e), which can be attributed to the introduction of the PEG trimethyl ammonium side chains. We studied with DFT (density function theory) calculations the electrostatic potential diagram of BTMAE–Vi (Figure S5) to better understand its increased solubility. The positively charged side chain induces a clear separation of electron-rich and electron-deficient regimes in BTMAE–Vi, increasing the molecular polarity and thereby improving solubility.

Then, the stability of BTMAE–Vi which significantly influences battery lifetime was systematically investigated, including the chemical stability, thermal stability, and electrochemical stability. ^{1}H NMR experiments reveal that the peak shift is unchanged after 150 days at room temperature or 60 °C (Figure S6), inferring the oxidized form of BTMAE–Vi is stable. The thermal stability of BTMAE–Vi is also analyzed by thermogravimetric analysis (TGA), demonstrating that BTMAE–Vi can withstand temperatures of up to 150 °C with no obvious mass loss (Figure S7). BTMAE–Vi was also cycled for 1000 continued CV cycles and the CV curves of BTMAE–Vi showed no significant change after 1000 cycles compared with the first CV cycle, showing good electrochemical stability (Figure S8).

To further qualify BTMAE–Vi as an anolyte candidate for AORFBs, the permeability of BTMAE–Vi was studied, using a two-compartment diffusion cell with a commercial Selemion DSV membrane. The permeability of BTMAE–Vi is $4.2 \times 10^{-11} \, cm^2 \, s^{-1}$, which is far lower than that of other viologen-based molecules[6–9,14] and is even two orders of magnitude slower than MV at $2.8 \times 10^{-9} \, cm^2 \, s^{-1}$ (Figures 1f, S9 and S10). Figure 1(g) shows that the membrane permeability of these viologen-based organics decreases with the increase of Van der Waal volume. Therefore, as expected, BTMAE–Vi possesses an extremely low permeability across the Selemion DSV membrane because of bigger molecular size and more positive charges.

After revealing its high solubility, fast kinetics, high stability and, low membrane permeability, we examined BTMAE–Vi in AORFB tests by pairing it with FcNCl catholyte[15] (schematic illustration is shown in Figure 2a). The redox potentials of BTMAE–Vi and FcNCl from cyclic voltammetry are shown together, −0.40 V and −0.74 V versus SHE for BTMAE–Vi and 0.61 V versus SHE for FcNCl (Figure 2b). The cell would have an open circuit voltage (OCV) of 1.03 V if only the first redox step of BTMAE–Vi was used. When the second redox reaction of BTMAE–Vi is involved, the cell voltage can increase to 1.37 V. Then a practical cell was assembled, with the anolyte comprising 10 mL of 75 mM BTMAE–Vi in 1 M NaCl, the catholyte comprising 30 mL of 100 mM FcNCl in 1 M NaCl, and
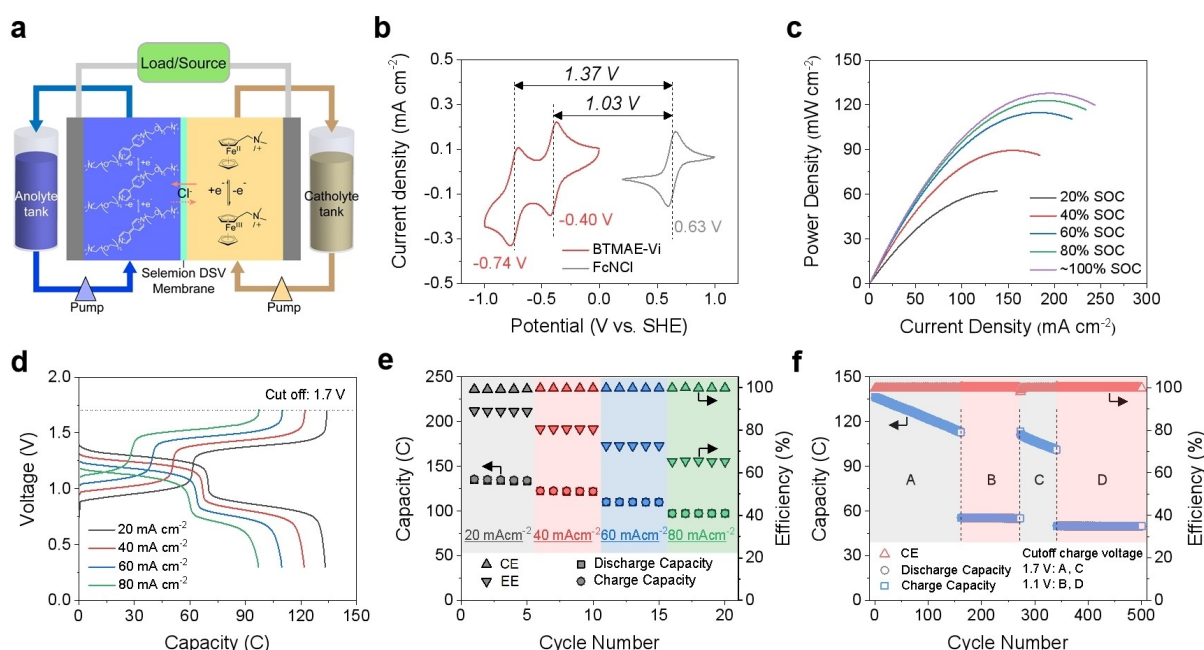

Figure 2. a) Schematic illustration of a pH-neutral FcNCl/BTMAE–Vi AORFB. b) Cyclic voltammograms of BTMAE–Vi (red trace), and FcNCl (gray trace). The experiment is conducted with 1.0 mM BTMAE–Vi or FcNCl in 1.0 M NaCl solution at a scan rate of 100 mV s^{-1}, on a glassy carbon working electrode (the arrowed lines indicate theoretical cell potentials). c) The polarization curves of the FcNCl/BTMAE–Vi cell measured at varied states of charge (SOCs). d) Charge and discharge curves collected at different current densities for the FcNCl/BTMAE–Vi cell; e) the discharge capacity, charge capacity, Coulombic efficiency (CE), and energy efficiency (EE) of the FcNCl/BTMAE–Vi cell when galvanostatically cycled at different current densities. Five repeated charge-discharge cycles are conducted for each current density. f) Extended cycling at 40 mA cm^{-2} of the flow cell with the same discharging cutoff voltage (0.3 V), but different charging cutoff voltages. For A and C periods, the charging cutoff voltage is 1.7 V. The charging cutoff voltage is 1.1 V for B and D periods. For cell cycling experiments, the anolyte is composed of 10 mL of 75 mM BTMAE–Vi in 1 M NaCl and the catholyte comprises 30 mL of 100 mM FcNCl in 1 M NaCl.

a Selemion DSV membrane transferring anions. The excess of FcNCl permits us to focus on the performance of the anolyte. The peak power density curves were collected at different SOCs and show a peak power density of 127.8 mW cm^{-2} at ~100% SOC (Figure 2c), which is higher than the MV/FcNCl[15] and BTMAP–Vi/FcNCl[16] cells. Rate performance of the BTMAE–Vi/FcNCl cell was investigated by operating the cell at increasing current densities from 20 to 80 mA cm^{-2} (Figure 2d and e). The charge-discharge cycles all display two plateaus because of the two redox processes of BTMAE–Vi. For each current density, a nearly constant cell capacity and Coulombic efficiencies of >99.2% are observed over the five cycles. The energy efficiency decreases from 88.9% at 20 mA cm^{-2} to 65.5% at 80 mA cm^{-2}, which is ascribed to the increased cell overpotential at high current densities.

To evaluate the cycling stability of the FcNCl/BTMAE–Vi cell, an extended galvanostatic cycling was performed at 40 mA cm^{-2} (Figure 2f). A potential hold was applied at cutoff voltages until the current density fell below 4 mA cm^{-2}. During the whole charge-discharge process, the Coulombic efficiency of the FcNCl/BTMAE–Vi cell maintains >99.2%. When the charging cutoff voltage was set to 1.7 V and discharging cutoff voltage was set to 0.3 V, two electrons storage capability of BTMAE–Vi was achieved. The cell retains 82.8% of the initial capacity after 160 cycles, indicating a capacity retention rate of 99.893% per cycle. When we decreased the charging cutoff voltage to 1.1 V, only first-electron redox process of BTMAE–Vi was involved. The capacity retention rate increases to 99.992% per cycle over 110 cycles, which is significantly higher than the previous charge-discharge process. Subsequently, we switched the charging cutoff voltage to 1.7 V and then 1.1 V, and obtained the reproducible results of the fade rates. Obviously, decreasing the charging cutoff voltage, which forces BTMAE–Vi to undergo the first redox process, significantly increases the capacity retention rate. And it is worth noting that the energy efficiency is higher with the charging cutoff voltage of 1.7 V (Figure S11).

To better understand the reason for capacity fade, postmortem cell analysis, symmetric cell cycling,[17] and computational simulations were performed. First, the anolyte and catholyte solutions after cycling were thoroughly studied by CV and ^{1}H NMR to detect possible membrane crossover or molecular degradation. CV voltammograms of catholyte and anolyte of the FcNCl/BTMAE–Vi cell after cycling are shown in Figure 3(a). The CV curve of the catholyte shows that the crossover of BTMAE–Vi through the Selemion DSV membrane is negligible owing to the big molecular size and the high number of positive charges. However, the crossover of FcNCl to the anolyte solution is observed. Besides catholyte crossover, unexpected proton signals are detected in the anolyte solution after cycling, implying that side reactions occurred for the electrochemically reduced BTMAE–Vi (Figures S12 and S13). Symmetric cell cycling was used to investigate the electrochemical stability of the reduced BTMAE–Vi (Figure 3b). At first, the potential limit was set to ±200 mV and BTMAE–Vi only used the first-electron to store electricity. The cell capacity remains unchanged, suggesting that the singly reduced BTMAE–Vi is electrochemically stable. However, when the potential limit was raised to ±500 mV, the capacity began to fade slowly. The capacity fade is ascribed to the access to the second electron reduction. Finally, the nucleus independent chemical shift (NICS) calculations[18] were conducted on the electronic structures of three redox states of BTMAE–Vi (Figure 3c). Note that the molecular aromaticity increases as the NICS value decreases.[19] The NICS values of two aromatic rings of BTMAE–Vi are −24.79 ppm and −23.66 ppm, respectively. And the NICS values become −5.14 ppm and −4.06 ppm after BTMAE–Vi is singly reduced, indicating the acceptance of one electron decreases the aromaticity. When BTMAE–Vi is doubly reduced, the NICS values increase to 11.74 ppm and 12.15 ppm, which are anti-aromatic, suggesting the poor stability. Therefore, we conclude the capacity fade of the FcNCl/BTMAE–Vi cell is mainly attributed to the irreversible molecular decomposition of the doubly reduced BTMAE–Vi.

To facilitate practical applications, a slightly concentrated FcNCl/BTMAE–Vi cell was constructed with 0.5 M BTMAE–Vi as anolyte and 0.5 M FcNCl as catholyte. The 0.5 M FcNCl/BTMAE–Vi cell has a peak power density of 140 mW cm^{-2} at ~100% SOC (Figure 4a). The charging cutoff voltage was set to 1.1 V, thereby not involving the second redox process (Fig-
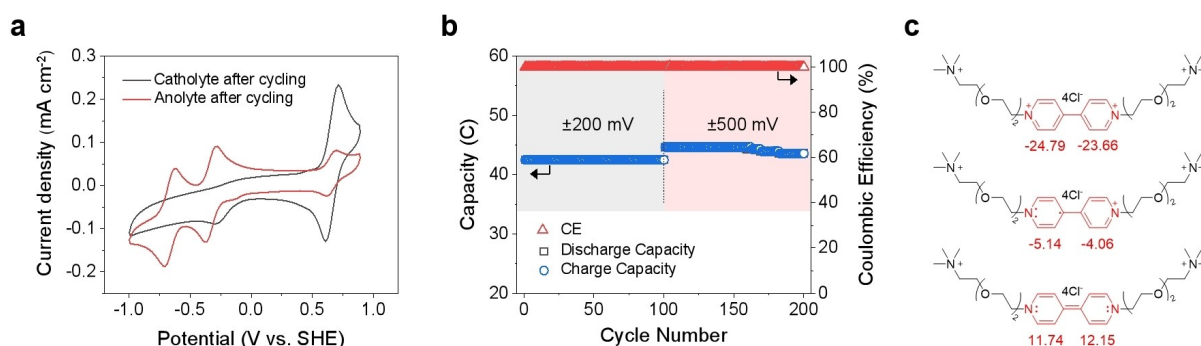

Figure 3. a) Cyclic voltammograms of catholyte (gray trace) and anolyte (red trace) of the FcNCl/BTMAE–Vi cell after cycling. b) Unbalanced compositionally symmetric cell cycling of BTMAE–Vi. As a capacity limiting side (CLS), 5 mL of 0.1 M BTMAE–Vi at 50% SOC in 1 M NaCl is placed in one reservoir of a flow cell and 8 mL of the same electrolyte is placed in the other reservoir as a non-capacity limiting side (NCLS). The cell is cycled potentiostatically between ±200 and ±500 mV. c) the nucleus independent chemical shift (NICS) values of BTMAE–Vi, singly reduced BTMAE–Vi and doubly reduced BTMAE–Vi.
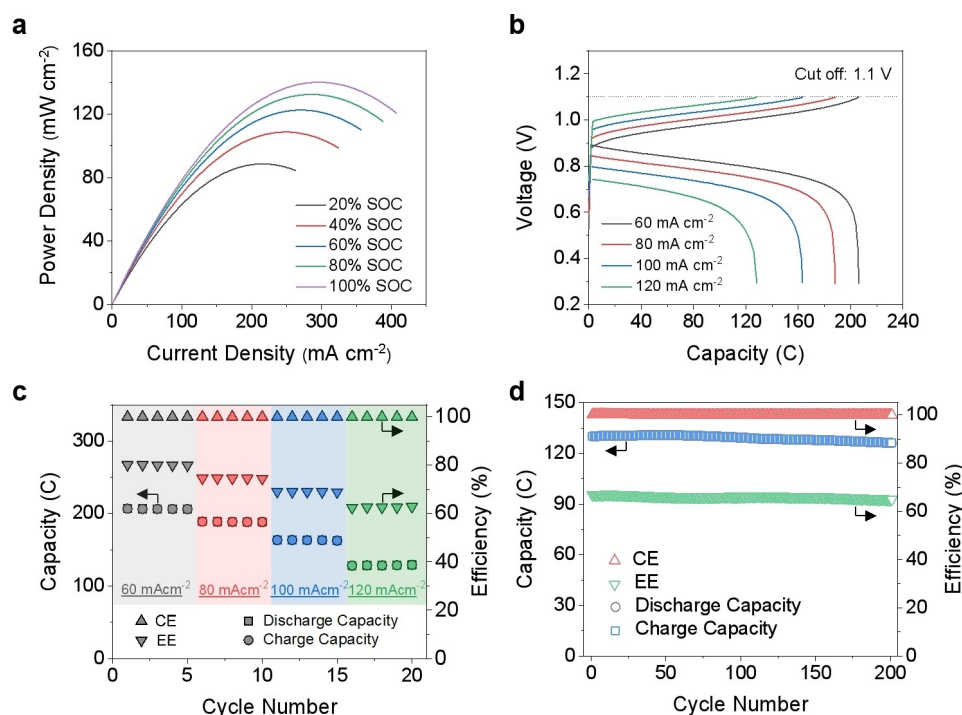
Figure 4. a) Polarization curves of a 0.5 M FcNCl/BTMAE–Vi cell measured at varied SOCs. The cell is charged at a potential of 1.1 V that only access the first redox reaction. b) Charge-discharge curves collected at varied current densities for the 0.5 M FcNCl/BTMAE–Vi cell. c) Discharge capacity, charge capacity, Coulombic efficiency (CE), and energy efficiency (EE) of the 0.5 M FcNCl/BTMAE–Vi cell galvanostatically cycled at varied current densities. d) Extended galvanostatic cycling of the 0.5 M FcNCl/BTMAE–Vi cell at 120 mA cm^{-2}. The entire 201 cycles occur over a period of 37.6 h. The anolyte comprises 5 mL of 0.5 M BTMAE–Vi and 1.0 M NaCl while the catholyte comprises 10 mL of 0.5 M FcNCl and 1.0 M NaCl. The cutoff voltages are 1.1 V and 0.3 V, and a potential hold is applied until the current density falls below 4 mA cm^{-2}. The cell is assembled with a Selemion DSV membrane.

ure 4b). When galvanostatically cycled at varied current densities of 60, 80, 100 and 120 mA cm^{-2}, the cell shows high Coulombic efficiency ($>$99.9%) and energy efficiency ($>$62.4%), as shown in Figure 4c. For extended galvanostatic cycling of the 0.5 M FcNCl/BTMAE–Vi cell at 120 mA cm^{-2}, a capacity retention rate of 99.996% per cycle or 99.979% per hour is manifested (Figure 4d). The FcNCl/BTMAE–Vi cells assembled with 1.0 M and 2.0 M BTMAE–Vi are also demonstrated in Figures S14 and S15, respectively. We did not go to higher concentrations primarily due to an increased viscosity of the anolyte, presumably induced by the reduced BTMAE–Vi.[9b] As the concentration of BTMAE–Vi increases, its long-term cycling stability is reduced dramatically. Generally, viologen radicals can undergo a dimerization degradation process.[7a] The reduced stability is probably because introducing the flexible polyethylene oxide trimethyl ammonium side chain does not mitigate dimerization. The electrochemical properties of BTMAE–Vi and reported viologen-based derivatives and their performance in AORFBs are summarized in Table S1. The cycling stability of BTMAE–Vi is inadequate compared with other reported viologen electrolyte systems, especially at high electrolyte concentrations. Although further work is still required to solve stability issues, we establish a strategy that could promote the development of crossover-free and high-capacity AORFBs.

Conclusion

In summary, we synthesize a viologen-based anolyte, BTMAE–Vi, for pH-neutral AORFBs, and establish a strategy that increases the molecular size, positive charges, and the polarity of redox-active organic molecules by introducing polyethylene oxide trimethyl ammonium side chain, thereby significantly mitigating membrane crossover issues and improving water solubility. The 0.5 M FcNCl/BTMAE–Vi cell demonstrates a high capacity retention rate of 99.996% per cycle or 99.979% per hour, when only the first one-electron redox process is involved. The anolyte material and the proposed concept may be broadly used for large-scale and high-performance energy storage applications.

Experimental Section

Materials

4,4'-bipyridine, trimethylamine (TMA) tetrahydrofuran solution, (ferrocenylmethyl)dimethylamine, methyl chloride, 1,2-bis(2-chloroethoxy)ethane ether, anhydrous acetonitrile, methyl tert-butyl ether (MTBE), anhydrous N,N-dimethylformamide (DMF), ethanol and sodium chloride (NaCl) were all purchased from Energy Chemical Co., Ltd. (Shanghai, China), and used as received without further purification. Throughout the study, deionized water was used.

Batteries & Supercaps

Research Article
doi.org/10.1002/batt.202200426

Chemistry Europe
European Chemical
Societies Publishing

^{1}H NMR spectroscopy

AVANCE III HD 400 spectrometers were used to record ^{1}H NMR spectra. ^{1}H NMR spectra for the cycled electrolytes were collected by directly diluting 100 μL of electrolytes in 700 μL of D_2O.

Synthesis of BTMAE-Vi

1,2-bis (2-chloroethoxy) ethane ether (7.44 g, 40 mmol) and TMA tetrahydrofuran solution (10 mL, 20 mmol) were added to a round-bottom flask. The resulting mixture was stirred at 60 °C for 72 h, which was then cooled to room temperature and diluted with ~50 mL of MTBE. The suspended white solid was collected by vacuum filtration and added to 50 mL acetone. The filtrate was collected by vacuum filtration. After drying the filtrate under reduced pressure, a pale yellow viscous liquid of 2-(2-(2-chloroethoxy)ethyl)-trimethyl-ammonium chloride (3.94 g, 40.1%) was obtained. In anhydrous DMF (~12 mL), 2.3 g (9.4 mmol) of 2-(2-(2-chloroethoxy)ethoxy)-trimethyl-ammonium chloride and 0.48 g (3.1 mmol) of 4,4'-bipyridine were heated to reflux under Ar. After heating for 72 h, the reaction mixture was cooled to room temperature. A grey solid was separated by vacuum filtration and washed several times with acetone, and vacuum dried to afford BTMAE–Vi (0.67 g, 33.3%). ^{1}H NMR (400 MHZ, D_2O): δ 9.04 (d, 4 H), 8.48 (d, 4 H), 4.84 (t, 4 H), 4.02 (t, 4 H), 3.86 (m, 4 H), 3.62 (m, 8 H), 3.49 (t, 4 H), 3.08 (s, 18 H).

Synthesis of FcNCl

The synthesis of FcNCl was conducted according to a previous report.[15] In a 250 mL flask, 30 mmol methyl chloride, 25 mmol (ferrocenylmethyl)dimethylamine, and 40 mL of anhydrous acetonitrile were mixed and then stirred continuously at room temperature overnight under Ar. A reddish-orange precipitate was separated by vacuum filtration and washed several times with ether. Finally, the product was dried under a vacuum and stored in a dry desiccator. ^{1}H NMR (400 MHZ, D_2O): δ 2.91 (s, 9 H), 4.19 (s, 5 H), 4.30 (s, 2 H), 4.35 (s, 2 H), 4.42 (d, 2 H).

Solubility and permeability measurements

The solubility of BTMAE–Vi was measured by dissolving the solid in water until producing precipitation. Then we diluted the viscous red solution by a known factor and calibrated the concentration of the diluted solution by UV-Vis (Persee, TU-1901, spectrophotometer) using a pre-established absorbance-concentration curve.

A lab-made two-compartment diffusion cell was used to evaluate the permeability of BTMAE–Vi and other viologen derivatives across the Selemion DSV membrane.[20] As exemplified with BTMAE–Vi, to the donating and receiving sides, 0.1 M BTMAE–Vi in 1.0 M NaCl aqueous solution and 1.4 M NaCl aqueous solution with the same volume were filled, respectively. Both solutions were continuously stirred. Aliquots were taken from the receiving side at different time intervals, diluted, and characterized using UV-Vis spectrophotometer. The concentration of BTMAE–Vi was calculated according to the calibration curve. The permeability coefficient P was calculated as follow.

$$P = \ln(1 - 2c_t/c_0)(-V_0 L/2A)/t$$

where P is the permeability coefficient, t is time, c_t is the concentration of BTMAE–Vi in the receiving side at t, c_0 is the initial concentration of BTMAE–Vi in the donating side, V_0 is the volume

of the solution in either compartment, L is the thickness of the membrane, and A is the membrane area.

Cyclic voltammetry (CV) studies

All CV studies were carried out using a ZENNIUM E electrochemical workstation (ZAHNER, Germany), with a glassy carbon (3 mm diameter) working electrode, an Ag/AgCl reference electrode (equilibrated with 3 M NaCl) and a platinum coil counter electrode. The glassy carbon electrode was polished with alumina slurry (0.5 μm) and rinsed with deionized water prior to measurement.

Rotating disk electrode (RDE) measurements

RDE measurements were conducted using a CHI600E potentiostat (CH Instruments, Inc., Austin, US) and a Pine E4TQ RDE, with a glassy carbon (5 mm diameter) rotating electrode, an Ag/AgCl reference electrode (equilibrated with 3 M NaCl) and a platinum coil counter electrode. Linear sweep voltammetry (LSV) scans from −0.2 to −0.9 V (vs. SHE) at a scan rate of 10 mVs^{-1} were recorded for BTMAE–Vi, with rotating speeds between 100 and 2500 rpm. Three repeated measurements ensured reproducible results. Background scans with 1.0 M NaCl aqueous solution were taken and subtracted. A Levich plot of the limited currents (i_{lim}) as a function of the square root of the rotating speeds (ω) was constructed. The diffusion coefficient D of BTMAE–Vi was calculated from the slope of the linear fitting using the Levich equation.[21]

$$i_{lim} = 0.620 nFAcD^{(2/3)} \nu^{(-1/6)} \omega^{(1/2)}$$

where n is number of electrons, F is Faraday constant, A is the electrode area, c is the concentration of BTMAE–Vi, ν is the kinematic viscosity of 1.0 M NaCl aqueous solution.

The mass-transfer-independent kinetic current (i_k) was provided by the Koutechy-Levich equation.

$$i^{-1} = i_k^{-1} + \left(0.620 nFAcD^{(2/3)} \nu^{(-1/6)} \omega^{(1/2)} \right)^{-1}$$

The Tafel equation[22] relating i_k for reducing electrolytes to the overpotential (η), was used to deduce the rate constant (k_0) as follow.

$$\log_{10}(i_k) = \log_{10}(nFcAk_0) + \alpha nF\eta/2.303RT$$

where α is the transfer coefficient, R is molar gas constant, and T is the operating temperature.

Full cell tests

Cell hardware was purchased from Fuel Cell Tech (Albuquerque, US). POCO sealed graphite flow plates with serpentine flow fields were used on both sides. The electrode on each side consisted of 3 stacked sheets of Sigracet SGL 39AA carbon paper electrodes (baked at 400 °C for 24 h prior to use) with 5 cm^2 geometric area. In all cases, the cell was assembled with a Selemion DSV membrane. The electrolytes were pumped through the cell stack at a flow rate of 60 rpm using a Masterfles L/S peristaltic pump (Cole-Parmer, Vernon Hills, IL). All tubing and electrolyte reservoirs were made from chemically resistant fluorinated ethylene propylene (FEP). Polarization and galvanostatic cell cycling were performed in a glovebox with oxygen level of <2 ppm on a Bio-Logic BCS-815 electrochemical workstation.

© 2022 Wiley-VCH GmbH

Batteries & Supercaps

Research Article
doi.org/10.1002/batt.202200426

Chemistry Europe
European Chemical
Societies Publishing

Computational calculations

DFT calculations were performed using Gaussian 16 program at B3LYP/6-311+G (d) level.[23] Vibrational frequency calculations were used to validate all minimized structures. Multiwfn, a multifunctional wavefunction analyzer developed by the Beijing Kein Research Center for Natural Sciences, was used to analyze the Van der Waals volume, electrostatic potential diagram, and NICS(1) zz value.[24]

Acknowledgements

Conflict of Interest

The authors declare no conflict of interest.

Data Availability Statement

The data that support the findings of this study are available from the corresponding author upon reasonable request.

[1] a) Z. Yang, J. Zhang, M. C. W. Kintner-Meyer, X. Lu, D. Choi, J. P. Lemmon, J. Liu, *Chem. Rev.* **2011**, *111*, 3577–3613; b) B. Dunn, H. Kamath, J.-M. Tarascon, *Science* **2011**, *334*, 928–935; c) W. S. Yang, B.-W. Park, E. H. Jung, N. J. Jeon, Y. C. Kim, D. U. Lee, S. S. Shin, J. Seo, E. K. Kim, J. H. Noh, S. I. Seok, *Science* **2017**, *356*, 1376–1379; d) N. Arora, M. I. Dar, A. Hinderhofer, N. Pellet, F. Schreiber, S. M. Zakeeruddin, M. Grätzel, *Science* **2017**, *358*, 768–771; e) G. C. Sedenho, D. De Porcellinis, Y. Jing, E. Kerr, L. M. Mejia-Mendoza, Á. Vazquez-Mayagoitia, A. Aspuru-Guzik, R. G. Gordon, F. N. Crespilho, M. J. Aziz, *ACS Appl. Energ. Mater.* **2020**, *3*, 1933–1943.
[2] a) W. Yan, C. Wang, J. Tian, G. Zhu, L. Ma, Y. Wang, R. Chen, Y. Hu, L. Wang, T. Chen, *Nat. Commun.* **2019**, *10*, 1–11; b) T. Janoschka, N. Martin, U. Martin, C. Friebe, S. Morgenstern, H. Hiller, M. D. Hager, U. S. Schubert, *Nature* **2015**, *527*, 78–81; c) Y. Li, L. Liu, C. Liu, Y. Lu, R. Shi, F. Li, J. Chen, *Chem* **2019**, *5*, 2159–2170.
[3] a) J. Luo, B. Hu, M. Hu, Y. Zhao, T. L. Liu, *ACS Energy Lett.* **2019**, *4*, 2220–2240; b) T. Janoschka, N. Martin, M. D. Hager, U. S. Schubert, *Angew. Chem. Int. Ed.* **2016**, *55*, 14427–14430; *Angew. Chem.* **2016**, *128*, 14639–14643; c) Y. Ding, C. Zhang, L. Zhang, Y. Zhou, G. Yu, *Chem. Soc. Rev.* **2018**, *47*, 69–103; d) Z. Li, Y.-C. Lu, *Adv. Mater.* **2020**, *32*, 2002132; e) Y. Liu, Q. Chen, P. Sun, Y. Li, Z. Yang, T. Xu, *Mater. Today Energy* **2021**, 100634.
[4] L. Zhang, R. Feng, W. Wang, G. Yu, *Nat. Chem. Rev.* **2022**, *6*, 524–543.
[5] Q. Chen, Y. Lv, Z. Yuan, X. Li, G. Yu, Z. Yang, T. Xu, *Adv. Funct. Mater.* **2022**, *32*, 2108777.
[6] T. Liu, X. Wei, Z. Nie, V. Sprenkle, W. Wang, *Adv. Energy Mater.* **2016**, *6*, 1501449.
[7] a) B. Hu, Y. Tang, J. Luo, G. Grove, Y. Guo, T. L. Liu, *Chem. Commun.* **2018**, *54*, 6871–6874; b) X.-L. Lv, P. Sullivan, H.-C. Fu, X. Hu, H. Liu, S. Jin, W. Li, D. Feng, *ACS Energy Lett.* **2022**, *7*, 2428–2434.
[8] a) C. DeBruler, B. Hu, J. Moss, J. Luo, T. L. Liu, *ACS Energy Lett.* **2018**, *3*, 663–668; b) M. Hu, W. Wu, J. Luo, T. L. Liu, *Adv. Energy Mater.* **2022**, *12* 2202085.
[9] a) S. Jin, E. M. Fell, L. Vina-Lopez, Y. Jing, P. W. Michalak, R. G. Gordon, M. J. Aziz, *Adv. Energy Mater.* **2020**, *10*, 2000100; b) M. Gao, M. Salla, Y. Song, Q. Wang, *Angew. Chem. Int. Ed.* **2022**, *61*, e202208223.
[10] a) J. Huang, S. Hu, X. Yuan, Z. Xiang, M. Huang, K. Wan, J. Piao, Z. Fu, Z. Liang, *Angew. Chem. Int. Ed.* **2021**, *60*, 20921–20925; b) S. Hu, T. Li, M. Huang, J. Huang, W. Li, L. Wang, Z. Chen, Z. Fu, X. Li, Z. Liang, *Adv. Mater.* **2021**, *33*, 2005839; c) J. Chai, A. Lashgari, Z. Cao, C. K. Williams, X. Wang, J. Dong, J. J. Jiang, *ACS Appl. Mater. Interfaces* **2020**, *12*, 15262–15270; d) C. DeBruler, B. Hu, J. Moss, X. Liu, J. Luo, Y. Sun, T. L. Liu, *Chem* **2017**, *3*, 961–978; e) C. Caianiello, L. F. Arenas, T. Turek, R. Wilhelm, *Batteries & Supercaps* **2022**, e202200355; f) M. Huang, S. Hu, X. Yuan, J. Huang, W. Li, Z. Xiang, Z. Fu, Z. Liang, *Adv. Funct. Mater.* **2022**, *32*, 2111744; g) M. Pan, L. Gao, J. Liang, P. Zhang, S. Lu, Y. Lu, J. Ma, Z. Jin, *Adv. Energy Mater.* **2022**, *12*, 2103478; h) G. Tang, Y. Liu, Y. Li, K. Peng, P. Zuo, Z. Yang, T. Xu, *JACS Au* **2022**, *2*, 1214–1222.
[11] J. Winsberg, C. Stolze, A. Schwenke, S. Muench, M. D. Hager, U. S. Schubert, *ACS Energy Lett.* **2017**, *2*, 411–416.
[12] a) Z. Huang, J. Lee, D. Henkensmeier, R. Hempelmann, S. Kim, R. Chen, *J. Electrochem. Soc.* **2020**, *167*, 160502; b) X. Yu, W. A. Yu, A. Manthiram, *ACS Appl. Mater. Interfaces* **2020**, *12*, 48654–48661.
[13] Z. Li, Y.-C. Lu, *Adv. Mater.* **2020**, *32*, 2002132.
[14] a) J. Luo, B. Hu, C. Debruler, T. L. Liu, *Angew. Chem. Int. Ed.* **2018**, *57*, 231–235; *Angew. Chem.* **2018**, *130*, 237–241; b) Y. Liu, Y. Li, P. Zuo, Q. Chen, G. Tang, P. Sun, Z. Yang, T. Xu, *ChemSusChem* **2020**, *13*, 2245–2249.
[15] B. Hu, C. DeBruler, Z. Rhodes, T. L. Liu, *J. Am. Chem. Soc.* **2017**, *139*, 1207–1214.
[16] E. S. Beh, D. De Porcellinis, R. L. Gracia, K. T. Xia, R. G. Gordon, M. J. Aziz, *ACS Energy Lett.* **2017**, *2*, 639–644.
[17] M.-A. Goulet, M. J. Aziz, *J. Electrochem. Soc.* **2018**, *165*, A1466-A1477.
[18] T. Lu, F. Chen, *J. Comput. Chem.* **2012**, *33*, 580–592.
[19] C. Zhang, Z. Niu, S. Peng, Y. Ding, L. Zhang, X. Guo, Y. Zhao, G. Yu, *Adv. Mater.* **2019**, *31*, 1901052.
[20] Y. Liu, M.-A. Goulet, L. Tong, Y. Liu, Y. Ji, L. Wu, R. G. Gordon, M. J. Aziz, Z. Yang, T. Xu, *Chem* **2019**, *5*, 1861–1870.
[21] B. Huskinson, M. P. Marshak, C. Suh, S. Er, M. R. Gerhardt, C. J. Galvin, X. Chen, A. Aspuru-Guzik, R. G. Gordon, M. J. Aziz, *Nature* **2014**, *505*, 195–198.
[22] P. Sun, Y. Liu, Y. Li, M. A. Shehzad, Y. Liu, P. Zuo, Q. Chen, Z. Yang, T. Xu, *Ind. Eng. Chem. Res.* **2019**, *58*, 3994–3999.
[23] M. J. Frisch, G. W. Trucks, H. B. Schlegel, G. E. Scuseria, M. A. Robb, J. R. Cheeseman, G. Scalmani, V. Barone, G. A. Petersson, H. Nakatsuji, X. Li, M. Caricato, A. V. Marenich, J. Bloino, B. G. Janesko, R. Gomperts, B. Mennucci, H. P. Hratchian, J. V. Ortiz, A. F. Izmaylov, J. L. Sonnenberg, Williams, F. Ding, F. Lipparini, F. Egidi, J. Goings, B. Peng, A. Petrone, T. Henderson, D. Ranasinghe, V. G. Zakrzewski, J. Gao, N. Rega, G. Zheng, W. Liang, M. Hada, M. Ehara, K. Toyota, R. Fukuda, J. Hasegawa, M. Ishida, T. Nakajima, Y. Honda, O. Kitao, H. Nakai, T. Vreven, K. Throssell, J. A. Montgomery Jr., J. E. Peralta, F. Ogliaro, M. J. Bearpark, J. J. Heyd, E. N. Brothers, K. N. Kudin, V. N. Staroverov, T. A. Keith, R. Kobayashi, J. Normand, K. Raghavachari, A. P. Rendell, J. C. Burant, S. S. Iyengar, J. Tomasi, M. Cossi, J. M. Millam, M. Klene, C. Adamo, R. Cammi, J. W. Ochterski, R. L. Martin, K. Morokuma, O. Farkas, J. B. Foresman, D. J. Fox, in, Wallingford, CT, **2016**.
[24] T. Lu, F. Chen, *J. Comput. Chem.* **2012**, *33*, 580–592.